J Mater Sci (2017) 52:674–685

Electrical properties of silica-doped 3 mol% yttria-stabilized tetragonal zirconia

Ewa Drożdż[1,*], Jan Wyrwa[1], Krystyna Schneider[2], and Mieczyslaw Rękas[1]

[1] *Faculty of Materials Science and Ceramics, AGH University of Science and Technology, al. A. Mickiewicza 30, 30-059 Krakow, Poland*

[2] *Faculty of Computer Science and Telecommunications, AGH University of Science and Technology, al. A. Mickiewicza 30, 30-059 Krakow, Poland*

Received: 25 May 2016
Accepted: 1 September 2016
Published online: 15 September 2016

ABSTRACT

Inconsistent opinions in the literature on the impact of silica on the conductivity of Y_2O_3–ZrO_2 system become a motivating reason to reinvestigate this matter. Too low a value of the grain boundaries' conductivity in the case of 3YSZ (3 mol% yttria-stabilized zirconia) is a fundamental barrier to using this material in the solid oxide fuel cell technology. The presence of silica is considered as the main cause of blocking effect on grain boundaries. The main purpose of this study involved the synthesis of nanomaterials, 3YSZ, with the addition of restricted amounts of silica. Two series of samples were prepared and sintered at the temperatures of 1073 and 1473 K. Then the obtained materials were tested for their phase composition, microstructure and electrical properties (based on analysis of the impedance spectra). The SEM microphotograph analysis indicated the decrease in the grain sizes of zirconia with the addition of SiO_2. Moreover, X-ray diffraction measurements showed the beginning of formation of zirconium silicate at 1473 K. The detailed investigation of microstructures and electrical properties shows that the two factors reported in the literature have an influence on grain boundary conductivity—grains sizes and the amount of introduced silica. Presented studies shows that up to temperature in which silica reacts with zirconia to form zircon ($ZrSiO_4$), its presence actually improves the grain boundaries conductivity due to decrease in particle size of YSZ (pinning effect). The blocking effect of silica at the grain boundaries begins to play a greater role causing the formation of glassy layers at a higher temperature.

Introduction

Zirconia-based materials are one of the first well-known oxygen-conducting solid electrolytes belonging to the Y_2O_3–ZrO_2-based solid solutions. Depending on the amount of Y_2O_3 additives used as a stabilizing agent, the appropriate crystallographic forms of zirconia are obtained. The three basic zirconia-type materials are considered the potential candidates by virtue of their extensive applications as

Address correspondence to E-mail: edrozdz@agh.edu.pl

DOI 10.1007/s10853-016-0361-2

engineering materials: fully stabilized zirconia (FSZ), partially stabilized zirconia (PSZ) and tetragonal zirconia polycrystals (Y-TZP). The fully stabilized zirconia has a cubic structure as a result of the introduction of 6–10 mol% Y_2O_3. This form exhibits high ionic conductivity at elevated temperatures, but its use is limited due to poor resistance to thermal shocks and low mechanical strength. Materials which contain 4–5 mol% Y_2O_3 (PSZ) consist of a mixture of cubic and tetragonal phases, which show good mechanical strength and toughness [1], but exhibit lower ionic conductivity than the fully stabilized system. The third-mentioned commercially used material has 1–3 mol% Y_2O_3 content (Y-TZP). This system has been found to have a submicron tetragonal grain structure [2, 3], mechanical strength (above 1GPa) and fracture toughness (>4–6 $MPa{\cdot}m^{1/2}$) [4, 5].

The *Yttria-Stabilized Zirconia* (the acronym for YSZ) is commonly used for the Y_2O_3–ZrO_2-based solid solutions, often taking into account the percentage of Y_2O_3 (e.g. 3YSZ, 10YSZ). Most discussed with regard to the applications—especially in the solid oxide fuel cells (SOFC) technology [6–8])—is 8YSZ; however, studies are still being conducted continuously for improving the properties of YSZ materials in order to overcome the previously mentioned disadvantages of this system. One way would be to use the appropriately modified tetragonal system (as 3YSZ) in applications that require higher conductivity; so far, the previous studies have only used the 8YSZ.

Badwal and Drennan [9] noticed that below 973 K, the grain interior of 3YSZ has higher conductivity (σ_b) than that of 8YSZ or a mixture of both tetragonal and cubic systems. The total conductivity of 3YSZ, however, is smaller than that of cubic zirconia, which is associated with the high contribution of grain boundary resistivity (known as the blocking effect) in the case of tetragonal system [10, 11]. According to Guo and Zhang [12], the specific grain boundary conductivity of YSZ systems is about two orders of magnitude lower than its bulk conductivity. In general, the literature cited two reasons for the blocking effect.

The first one is connected with the presence of impurities that are segregated on grain boundaries. The most common contaminant of zirconia is silica. According to some authors, SiO_2 can form a glassy layer that can completely cover zirconia grain [13], and subsequently oxygen ion transport across grain boundaries must proceed through this isolating layer [14]. Some other authors postulate only partial wetting of grain boundaries by silica [15] with some direct grain-to-grain contact. This description of the mechanism of silica influence leads to the conclusion that oxygen ion conduction takes place through direct contact between grains [16]. The formation of zirconium silicate by the reaction of ZrO_2 and SiO_2 nanopowders after 1 h of sintering even at 1473 K was confirmed by Pradhan and Sinha [17].

In contrast to the first thesis, Guo and Zhang [12] and Verkerk et al. [18] postulated the second reason for the blocking effect based on observation of yttrium cations' segregation [19] on the ZrO_2 grain boundaries. The mechanism of creation of the electrical potential at grain boundaries results in creation of a barrier (Schottky barrier) to the ion transport associated with the depletion of the positively charged oxygen vacancies on grain-to-grain contacts [20]. As shown [12], the grain boundary blocking effect reduces with the decreasing grain size due to the increasing concentration of oxygen vacancies.

So far, the reviews for these two pathways of electrical potential at grain boundaries are highly controversial. It should also be noted that, although silica is considered as detrimental to ionic conductivity, it can be used to achieve densification (during sintering) and for improving the superplastic properties of YSZ [21, 22]. In addition, in the case of the tetragonal phase, the addition of silica prevents the grain growth at critical sizes greater than ca. 0.3 μm, where tetragonal zirconia is unstable while transforming to the monoclinic phase.

As can be deduced from the above short review of the literature, the role of silica in YSZ materials is still controversial and yet to be resolved. Moreover, taking into account the promising application of the tetragonal zirconia, mainly as a solid electrolyte (in the form of dense body) and/or as a component of anode cermet material (in the form of porous material) in the intermediate temperature solid oxide fuel cells (IT-SOFC), the effects of the addition of silica on grain growth should be analysed. Thus, because the current study is focused on the analysis of dense materials, this work presents an analysis of the impacts of the addition of SiO_2 on properties (structural and electrical) of the porous 3YSZ materials.

Materials and methods

Sample preparation

The modified citric method was used in order to obtain series of samples with different compositions: first one, 3YSZ—3 mol% yttria-stabilized zirconia samples containing SiO_2 in various amounts—0.25, 0.5, 1.0 and 5.0 mass% SiO_2.

The saturated solutions of yttrium and zirconyl nitrates were prepared and mixed in proper ratio in order to obtain 3YSZ materials. All reagents used were analytically pure (provided by Sigma–Aldrich), and their compositions were analytically verified by classical chemical analysis (mass method). Next, the calculated amount of citric acid monohydrate (with 5 mol% excess) was added to the solution consisting of mixed nitrates. The resulting solution was left for a few hours on a hot plate (around 473 ± 5 K) to evaporate and then kept stirred. The final solution turned to grey–brown gel, which was afterward heated using the burner. In the next step, SiO_2 (POCH, analytically pure, with nanosized particle sizes in the range: 2–57 nm) was added to the prepared material. The mixture was ball milled for 16 h with isopropyl alcohol. Then it was calcined at 873 K for 1 h.

The materials containing 0–5 mass % of SiO_2 were pressed (under the pressure *c.a.* 5 10^5 Pa) and sintered at 1073 and 1473 K in air atmosphere for 3 h. On the other hand, the samples of 50 mol% 3YSZ–50 mol% SiO_2 were sintered at 1473 and 1673 K.

It should be noticed that the materials obtained with the described method, sintered at 1073 K, have high total porosity (the relevant table is given in Results section) as was obtained for the previously materials with the analogous method [23].

Structural and morphological characterizations

The phase composition of the products was determined by XRD analysis using a Philips X'Pert Pro diffractometer within the range of diffraction angles, 2θ, from 20 to 100 with monochromatized CuKα radiation. Crystallite sizes were determined from the X-ray line broadening of the selected peaks by means of the Scherrer approach.

Microstructural observations with chemical analysis were carried out using scanning electron microscopy (SEM) NOVA NANOSEM 200 (FEI Europe Company) coupled with X-ray energy dispersive spectroscopy (EDAX company apparatus). For morphological observations, the samples were polished and subsequently thermally etched at 1073 K for 1 h. Such a procedure allowed grain boundaries to be revealed and was useful for the determination of the grain size and shape. Relatively low etching temperature preserved the grain growth during this process. SEM images after binarization were processed using Image J 3.14 program. This analysis yielded the quantitative estimates of the grain size and shape.

Impedance spectroscopy

Before performing measurements of conductivity, Pt paste was applied as the electrode and fired at 1073 K for 2 h. The conductivities of 3YSZ pellets and 3YSZ-SiO_2 composites were measured in the atmosphere of 10 %H_2/90 %Ar mixture at different temperatures of 823, 873, 923, 973 and 1023 K. The electrical properties were examined by means of impedance spectroscopy using a computer-controlled Solartron (FRA 1260 and dielectric interface 1294). The impedance spectra were analysed using the ZPLOT software package provided by Solartron. The measurements were performed within the 0.1 Hz–1 MHz frequency range, and the amplitude of the sinusoidal voltage was set to 10 mV.

The impedance spectra were analysed using ZView software.

Results

Structural and microstructural characterizations

The X-ray diffraction analysis of the samples sintered at 1073 K (Fig. 1) revealed the presence of the tetragonal majority phase with a minor contribution of monoclinic phase (which is connected with incomplete stabilization of tetragonal phase in this temperature). The presence of reflexes corresponding to SiO_2, ZrO_2 cubic, $ZrSiO_4$ or Y_2O_3 phases was not observed. On the other hand, all peaks of the XRD of the samples containing 0.25–5 wt% of SiO_2 and sintered at 1473 K (Fig. 2a, b) can be assigned only to the tetragonal phase. The amounts of added SiO_2 in these

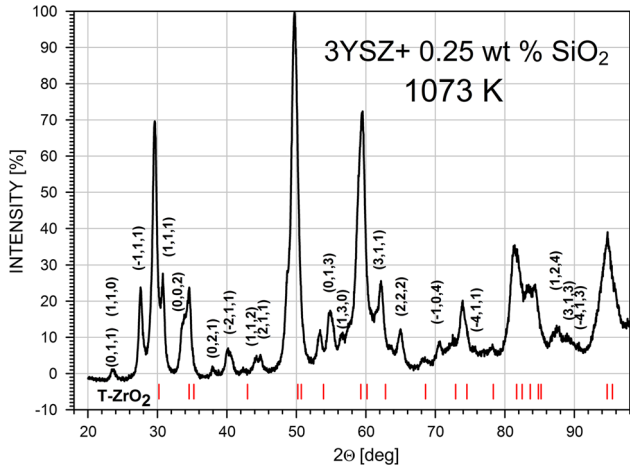

Figure 1 X-ray diffractogram of 3YSZ samples with 0.25 wt% SiO_2, sintered at 1073 K. The pattern of tetragonal phase is given at the *bottom* of the picture (T-ZrO_2). Reflections with their associated Miller indicators correspond to the monoclinic phase.

samples were too low to be identified, but there was also the possible formation of a glassy silica layer [13]. Moreover, for these samples, as in the case of low-temperature-sintered samples, $ZrSiO_4$ phase is not observed. Therefore, additional samples 3YSZ–SiO_2 with a large amount of silica (50 mol%) were synthesized. Figure 3a, b presents the XRD patterns of the sample 3YSZ + 50 mol% SiO_2 sintered at 1473 K (Fig. 3a) and 1673 K (Fig. 3b). As can be observed in the figure, especially in the case of the samples sintered at 1473 K, not only the presence of reflections originating from tetragonal ZrO_2 (3YSZ) and cristobalite is observed, but also the peaks corresponding to the zircon ($ZrSiO_4$) can be identified. The detailed analysis using Rietveld method indicated the amount of zircon to be 1.7 wt%. For the sample sintered at 1673 K, all the three phases—tetragonal ZrO_2, silica and tetragonal $ZrSiO_4$—can be clearly distinguished.

So far, the obtained results are consistent with those postulated by Pradhan and Sinha [17] despite the fact that the vast majority of authors have reported that zircon can be formed at temperatures above 1573 K. The presence of this phase in lower temperature can significantly affect the properties of 3YSZ–SiO_2 samples.

The determined values of the lattice constants of 3YSZ are compiled in Table 1. They are practically independent of the added amounts of SiO_2. They are 0.0025 nm—lattice constant *a* and 0.0019 nm—lattice constant *c*, higher than those of the existing literature

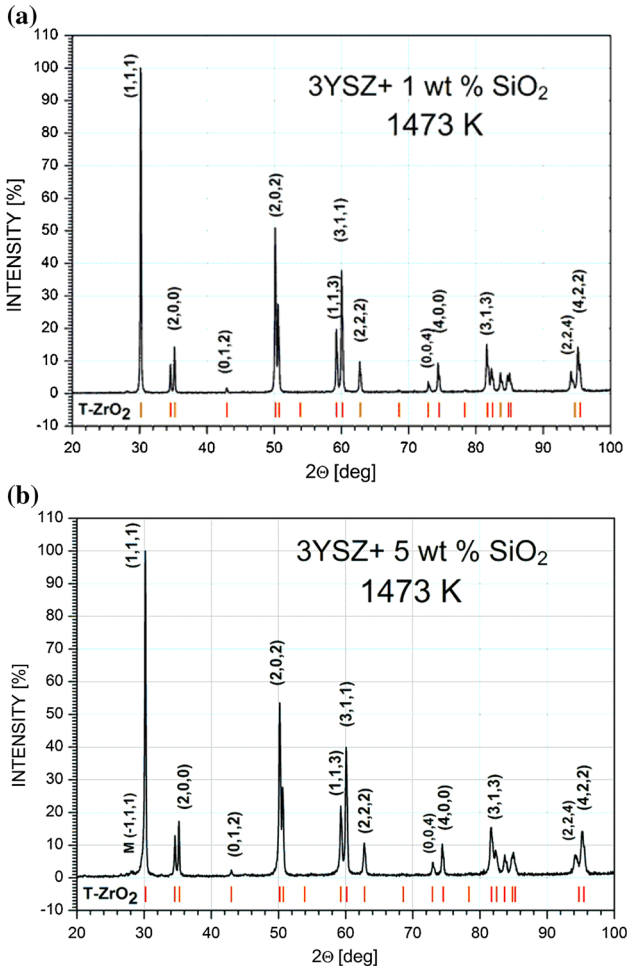

Figure 2 X-ray diffractograms of 3YSZ samples, sintered at 1473 K containing **a** 1.0 wt% SiO_2; **b** 5.0 wt% SiO_2. The Miller indicators were assigned to the corresponding reflexes. *M* monoclinic phase.

data for tetragonal zirconia [24–26]. These increased values of lattice constants can be interpreted as due to the substitution of zirconium ions (Zr^{4+}) by the bigger yttrium ions (Y^{3+}). According to Vegard's law, we can expect

$$\Delta x = (r_{Y3+} - r_{Zr4+}) * \frac{p}{100}, \quad (1)$$

where $\Delta x = a_{experimental\_3YSZ} - a_{tetrag\cdot ZrO_2} \approx c_{experimental\_3YSZ} - c_{tetrag\cdot ZrO_2}$, and r_{Y3+} and r_{Zr4+} are the ionic radii of yttrium and zirconium with coordination number equal to 8., and p is the atomic % of yttrium in zirconium sublattice. Taking into consideration the ionic radii, as reported by Shannon and Prewitt [27] of Y^{3+} and Zr^{4+}, of 0.1015 and 0.084 nm, respectively, we obtain from Eq. (1) that $\Delta x = 0.0020$ nm.

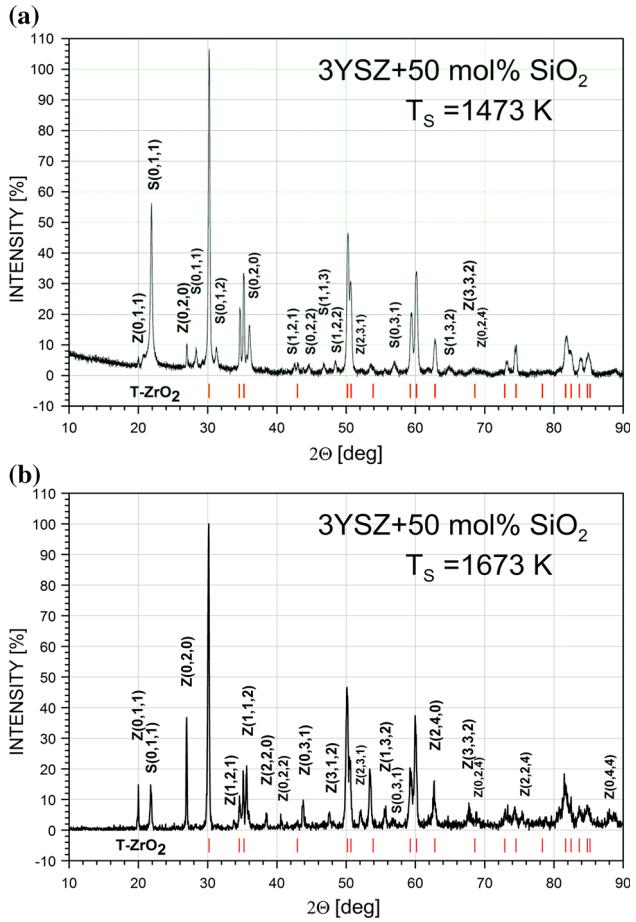

Figure 3 X-ray diffractograms of 3YSZ with 0.25 wt% SiO_2, sintered at **a** 1473 K; **b** 1673 K. Description of reflexes: zircon (Z), silica (S).

XRD patterns were used for determination of the crystallite size. Crystallite size (L) was calculated using Scherrer equation:

$$d = \frac{0.9\lambda}{\Delta(2\theta)\cos\theta}, \qquad (2)$$

where $\lambda = 0.154056$ nm is the X-ray wavelength; $\Delta(2\theta)$ is the broadening of the XRD peak at the half of its maximum intensity (FWHM); and θ is the Bragg angle. Parameter d was determined from the 3 to 5 peaks. Its mean value is presented in Table 1.

Samples sintered at 1073 K show smaller crystallite sizes than those of the samples after sintering at 1473 K (which results from the process beginning with grain growth at high temperature). On the other hand, the crystallite sizes of the samples sintered at 1473 and 1673 K are practically the same and independent of silica contents. Their mean value is $d_{mean} = 28.6 \pm 4.4$ nm. Crystallite size of $ZrSiO_4$ is about 40 nm.

Typical SEM micrographs of the samples 3YSZ and 3YSZ + 0.5 wt% SiO_2 sintered at 1473 K are presented in Fig. 4a, b, respectively. All the samples exhibit comparable grain structures. The average EDX analysis carried out during SEM observations confirmed the presence of silicon in all the samples except in the samples of pure 3YSZ.

The plot of the determined grain sizes versus SiO_2 concentrations on the basis of SEM microphotographs is presented in Fig. 5. The grain size decreased monotonously with the increasing silica content. This result is similar to that observed for the 8YSZ–SiO_2 samples [21]. It is caused by the grains' pinning effect due to intergranular silica. For comparison, in Fig. 6, a typical micrograph of the microstructures of the samples after heating at 1073 K is presented. The picture shows microstructure with the grain sizes of around 80 nm—about half the size of a grain observed in the case of samples sintered at 1473 K.

The total porosity values of the obtained materials determined on the basis of mass and geometric measurements are presented in Table 2. One can observe that, in the case of sample sintered at 1073 K, these values are comparable to each other, but for the sample sintered at 1473 K, these values considerably vary. The total porosity of samples sintered at 1473 K decreases with the amount of SiO_2 added, which confirms the densification effect of silica observed and the previously considered in the literature [21, 22].

Electrical properties

Figures 7 and 8 show examples of impedance spectra measured for 3YSZ at different temperatures in H_2/Ar atmospheres, for undoped 3YSZ sintered at 1073 and 1473 K, respectively. In this case, the separation of high-frequency region corresponding to the bulk properties and an intermediate-frequency region corresponding to the grain boundary properties can be distinguished for all presented temperatures. Two arcs are visible with clearly higher diameter of arc corresponding to grain boundary, which indicates the blocking properties of grain boundaries. The equivalent circuits presented in the both (Figs. 7, 8) pictures were used for fitting procedure, where R_1 and R_2 correspond to the resistances of CPE_1 and CPE_2, which are the non-Debye elements of grain interior and grain boundary, respectively.

Table 1 Crystallographic properties of the 3YSZ–SiO_2 samples

Sample	Lattice constants		Crystallite size (nm)	Figures/References
	a (nm)	*c* (nm)		
3YSZ Ts = 1073 K	0.5111	0.5201	9.8 ± 5.2	This work
3YSZ Ts = 1473 K	0.5097	0.5178	18.3 ± 7.1	This work
3YSZ + 0.25 wt% SiO_2 Ts = 1073 K	0.5115	0.5206	16.6 ± 13.5	This work (Fig. 1)
3YSZ + 1 wt% SiO_2 Ts = 1073 K	0.5128	0.5198	9.2 ± 2.3	This work
3YSZ + 0.25 wt% SiO_2 Ts = 1473 K	0.5096	0.5179	23.3 ± 5.5	This work
3YSZ + 1 wt% SiO_2 Ts = 1473 K	0.5096	0.5179	35.4 ± 4.6	This work
3YSZ + 5 wt% SiO_2 Ts = 1473 K	0.5094	0.5178	29.3 ± 6.5	This work (Fig. 2b)
3YSZ + 50 wt% SiO_2 Ts = 1473 K	0.5104	0.5175	26.3 ± 8.3	This work (Fig. 3a)
3YSZ + 50 wt% SiO_2 Ts = 1673 K 3YSZ phase	0.5102	0.5156	28.7 ± 5.1	This work (Fig. 3b)
3YSZ + 50 wt% SiO_2 Ts = 1673 K $ZrSiO_4$ phase	0.5832	0.5196	39.4 ± 11.6	This work (Fig. 3b)
Tetragonal ZrO_2 literature	0.5070	0.5160		[24]
	0.5094	0.5177		[25]
Tetragonal $ZrSiO_4$ literature	0.6580	0.5930		[26]

Bulk specific conductivity (σ_{bulk}) values were determined from the relation:

$$\sigma_{bulk} = \frac{l}{R_1 * S}, \quad (3)$$

where l is the thickness of the sample, and S is its cross-sectional area.

Similarly, total grain boundary conductivity ($\sigma_{Total,\ gb}$) values were determined from the relation:

$$\sigma_{Total,gb} = \frac{l}{R_2 * S}. \quad (4)$$

Both bulk (σ_{bulk}) and grain boundary ($\sigma_{Total,\ gb}$) conductivities can be analysed as thermally activated ionic transport and can be expressed as

$$\sigma = \frac{\sigma_o}{k_B T} \exp\left(-\frac{E_{act}}{k_B T}\right), \quad (5)$$

where k_B is the Boltzmann constant, and E_{act} is the activation energy.

Figure 9 shows electrical conductivities of 3YSZ in Arrhenius representation ($\log(\sigma T)$ vs. T^{-1}). The determined activation energies E_{act} are listed in Table 3 compared with the representative literature data [12, 18, 21, 28–31]. As shown in the table, the activation energies agree quite well to those of the tetragonal YSZ. The activation energy of the grain boundary conductivity is higher by about 15 % than those of the bulk. Some differences in electrical conductivity values and activation energies are observed between the samples sintered at 1073 and 1473 K. Based on the XRD analysis, we can conclude that the results of the sample sintered at 1473 K are more representative of the phase of tetragonal YSZ.

The specific grain boundary conductivity (σ_{gb}) is the average conductivity of the grain boundary and is given by [32]

$$\sigma_{gb} = \frac{\delta}{d} * \sigma_{Total,gb}, \quad (6)$$

where δ is the grain boundary thickness, d is the average grain size, and $\sigma_{Total,gb}$ is the total grain boundary conductivity which is calculated in respect

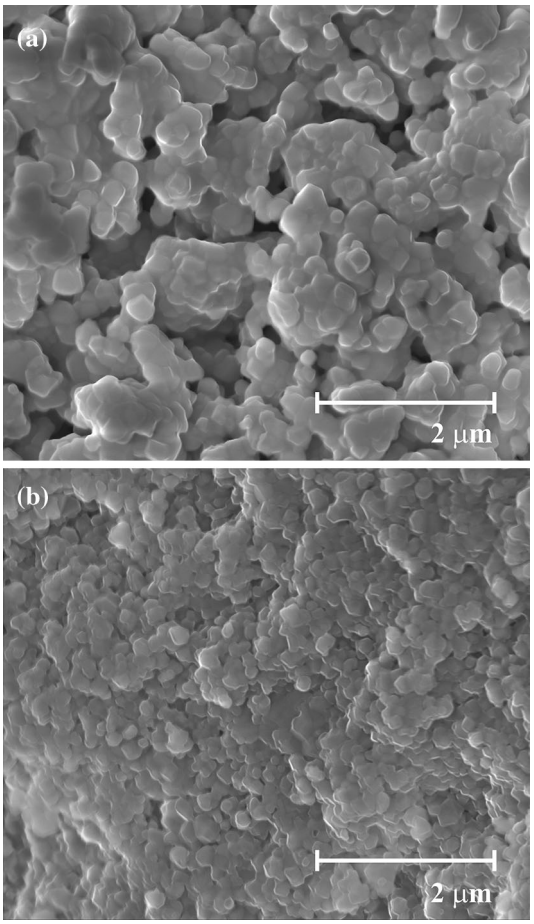

Figure 4 SEM analysis of samples: **a** 3YSZ; **b** 3YSZ + 0. 5 wt% SiO_2 sintered at 1473 K.

of the geometry of the sample and grain boundary resistance values obtained based on the EIS measurements.

Assuming equal values of the dielectric constant of the bulk and grain boundary (this assumption is commonly used in the literature), the grain boundary thickness can be determined from the impedance results using the relationship:

$$\delta_{gb} = d * \frac{C_{bulk}}{C_{gb}}, \tag{7}$$

where C_{bulk} and C_{gb} are the effective capacitances of the bulk and grain boundary, respectively. They may be calculated from the following relationship [33]:

$$C_i = (R_i^{n_i} A_i)^{\frac{1}{n_i}}, \tag{8}$$

where R_i represents the resistance of the bulk (i = 1) or grain boundary (i = 2), and A_i and n_i are the parameters of characterizing impedances of the CPE_i elements, $Z_{CPE:}$

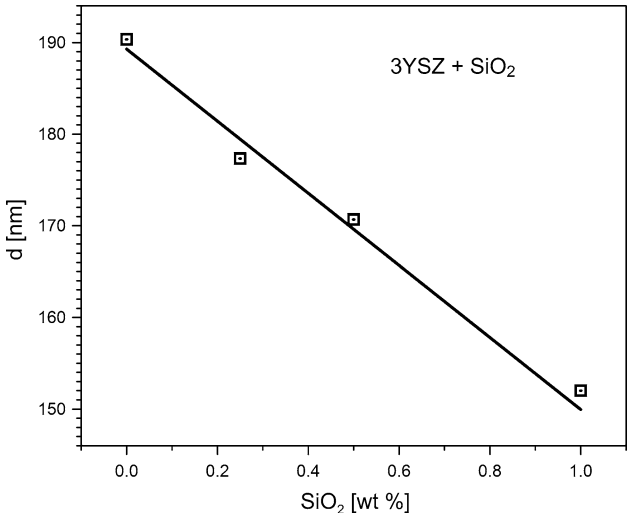

Figure 5 Grain size versus SiO_2 concentration for 3YSZ_SiO_2 samples sintered at 1200 °C.

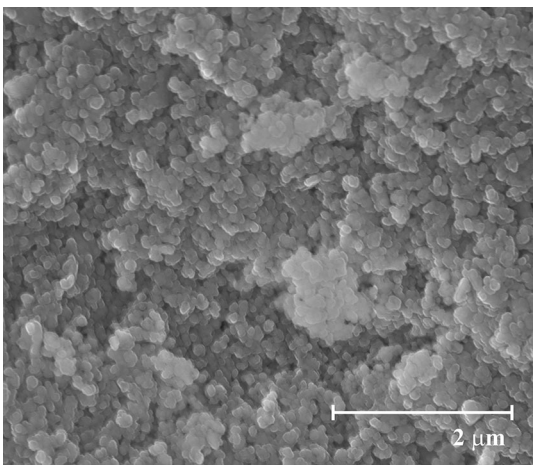

Figure 6 SEM microphotographs of 3YSZ + 0.5 wt% SiO_2 samples sintered at 1073 K.

$$Z_{CPE_i} = A_i^{-1}(j\omega)^{-n_i}, \tag{9}$$

where i = 1 corresponds to the bulk, and i = 2 corresponds to the grain boundary. The δ_{gb} estimated from the Eq. (7) is about (5.2 ± 1.1) nm. This value agrees with literature data for tetragonal YSZ materials: δ_{gb} = 4–6 nm reported by Ikuhara et al. [34]; δ_{gb} = 5.0 nm by Guo and Zhang [12]; δ_{gb} = 5 nm by Lee and Kim [35].

Dashed lines in Fig. 9 illustrate the specific grain boundary conductivities (σ_{gb}) of both samples sintered at 1073 K and 1473 K. The specific grain boundary conductivity was about 20 – 40 times lower than the bulk conductivity of the sample sintered at

Table 2 Total porosity values of the obtained samples

Sample	Total porosity [vol%]	
	Sintering temperature 1073 K	Sintering temperature 1473 K
3YSZ	56 ± 2	26 ± 2
3YSZ + 0.25 % SiO_2	54 ± 2	23 ± 2
3YSZ + 0.5 % SiO_2	54 ± 3	22 ± 2
3YSZ + 1 % SiO_2	53 ± 2	19 ± 2
3YSZ + 5 % SiO_2	50 ± 3	17 ± 2

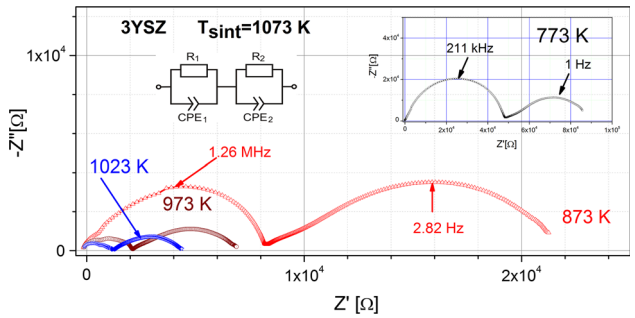

Figure 7 Nyquist plots of the impedance of 3YSZ sintered at 1073 K at several temperatures.

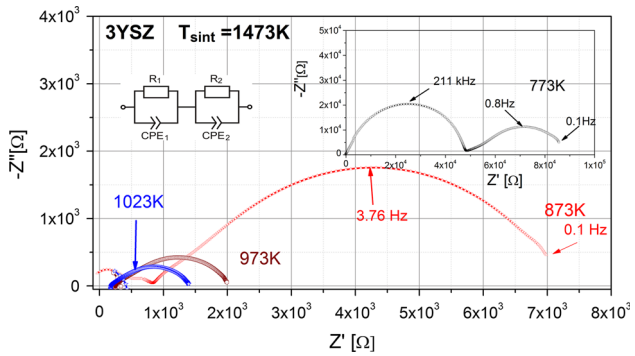

Figure 8 Nyquist plots of the impedance of 3YSZ sintered at 1473 K at several temperatures.

1473 K and 7–12 times lower than that of the sample sintered at 1073 K.

The effects of the added silica on the electrical conductivity grain boundary are presented in Fig. 10a, b. First of all, it can be observed that specific grain boundary conductivity for 3YSZ is higher for the samples sintered at 1073 K than for those sintered at 1473 K. This is consistent with expectations since two orders of magnitude smaller grains sizes of samples are obtained with modified citric method and sintered at 1073 K. Above about 1423 K, shrinkage of 3YSZ occurs, resulting in grain growth associated with the decrease of porosity and total length of grain boundaries. As a consequence, the specific

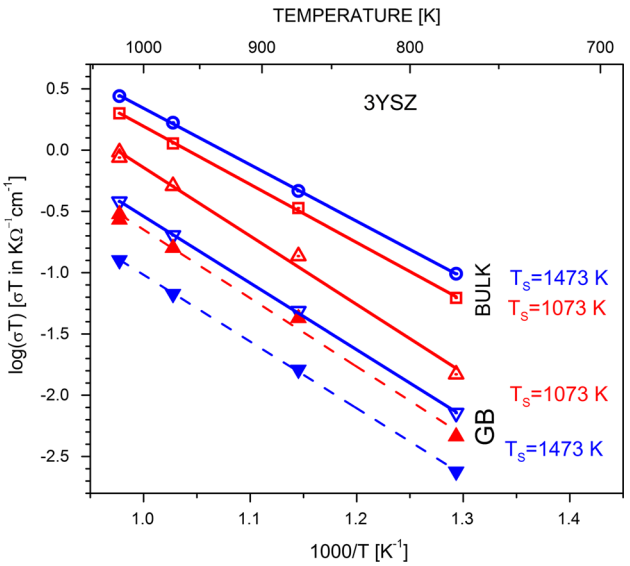

Figure 9 Temperature dependences of bulk and total/specific (*solid/dashed line*) grain boundary conductivities for 3YSZ samples sintered at 1073 and 1473 K.

grain boundary conductivity drops to lower values. With the increasing amount of silica addition from 0.25 to 1 wt%, the decreases of the electrical conductivities σ_{gb} are observed for both the series of samples. This effect agrees with the postulated formation of the insulating barrier layers. However, it needs to be highlighted that the smaller effect of the SiO_2 addition on the σ_{gb} of the samples sintered at 1473 K is noted than that in the case of samples sintered at 1073 K. Only the addition of larger SiO_2 amounts (5 wt%) for the sample sintered at 1473 K leads to a further reduction of specific grain conductivity value. A similar drop of σ_{gb} (by around one-and-a-half order of magnitude) for 3YSZ + 1.0 wt% SiO_2 sample sintered at 1073 K is observed.

It can be stated that the changes in the values of electrical conductivity of grain boundary of the samples sintered at 1473 K are the result of two effects: a decrease in grain sizes with the amount of introduced SiO_2 (Fig. 5) on the one hand and the

Table 3 The comparison of activation energies [eV] for YSZ materials

Sample	*E*a_b [eV]	*E*a_gb [eV]	References
8YSZ	1.175 ± 0.020	1.186 ± 0.020	[18]
1.7–2.9 YSZ	0.83 ± 0.03	1.03 ± 0.03	[28]
8YSZ	1.11−1.14	1.15−1.25	[21]
3YSZ	0.92	1.13	[12]
3YSZ, micro	0.92 ± 0.03	1.17 ± 0.03	[29]
3.3YSZ, SC	0.92 ± 0.04	–	[30]
2.8YSZ	–	1.22 ± 0.04	[31]
3YSZ, T_S = 1073 K	0.940 ± 0.01	1.108 ± 0.047	This work
3YSZ, T_S = 1473 K	0.914 ± 0.007	1.081 ± 0.011	This work

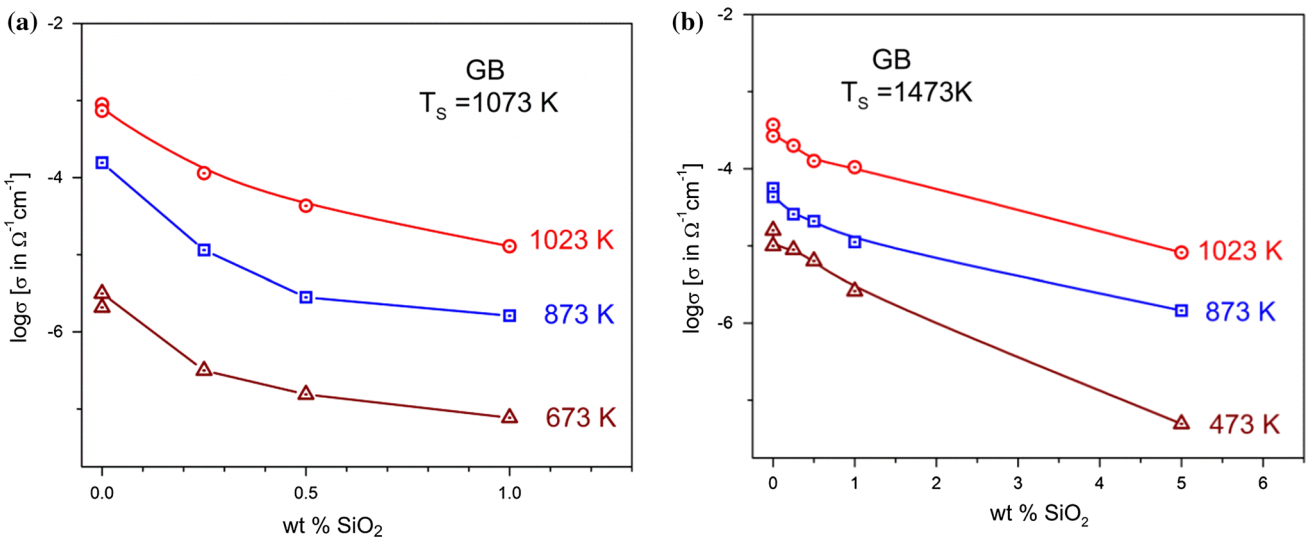

Figure 10 Electrical conductivities versus SiO_2 concentrations of the samples 3YSZ + xSiO_2 at 673, 873 and 1023 K: **a** σ_{gb} of the sample sintered at 1073 K; **b** σ_{gb} of the sample sintered at 1473 K.

beginning of $ZrSiO_4$ formation (Fig. 3a) on the other hand. The formation of compact, glassy insulating barrier at higher temperatures (as suggested by other authors) can affect the lowering of grain boundaries' conductivities in YSZ materials, but the results presented above prove that the contribution of this process should be even negligible (taking into account the results of XRD analysis). It seems that in the case of the presented materials, the effects of small-sized grains and their further decreasing with the SiO_2 addition (at the same time still having relatively a large porosity) produce the dominant influence on the reduction of σ_{gb}. As can be concluded, the Schottky barrier effect in the case of porous YSZ materials can overcome the negative influence related with the small contamination by silica. However, the introduction of the large amount of silica leads to a change in the conduction mechanism as a result of glass-layer formation around YSZ grains.

The dependences of activation energies for the grain interior (bulk) and the grain boundaries (gb) versus silica content are illustrated in Fig. 11a, b. As can be observed, for both series of materials, the dependences of the activation energy of grain boundaries' conductivities (E_{act_gb}) on the amount of SiO_2 are completely different. In the case of samples sintered at 1073 K, the E_{act_gb} values decrease with the SiO_2 addition (up to 0.5wt% of SiO_2) and then slightly increase for the 3YSZ + 1.0 wt% SiO_2 sample. It is worth noting that the introduction of already 0.25 wt% SiO_2 results in lower E_{act_gb} compared with pure 3YSZ. The other behaviour for the series of samples sintered at 1473 K is observed—first with the increasing the amount of SiO_2, the values of E_{act_gb} increase up to 0.5 wt% SiO_2 composition, and then decrease for the 3YSZ + 1.0 wt% SiO_2 and 3YSZ + 5.0 wt% SiO_2 samples. The nature of changes in the values of E_{act_gb} in both series of samples indicates different impacts of the additive on the

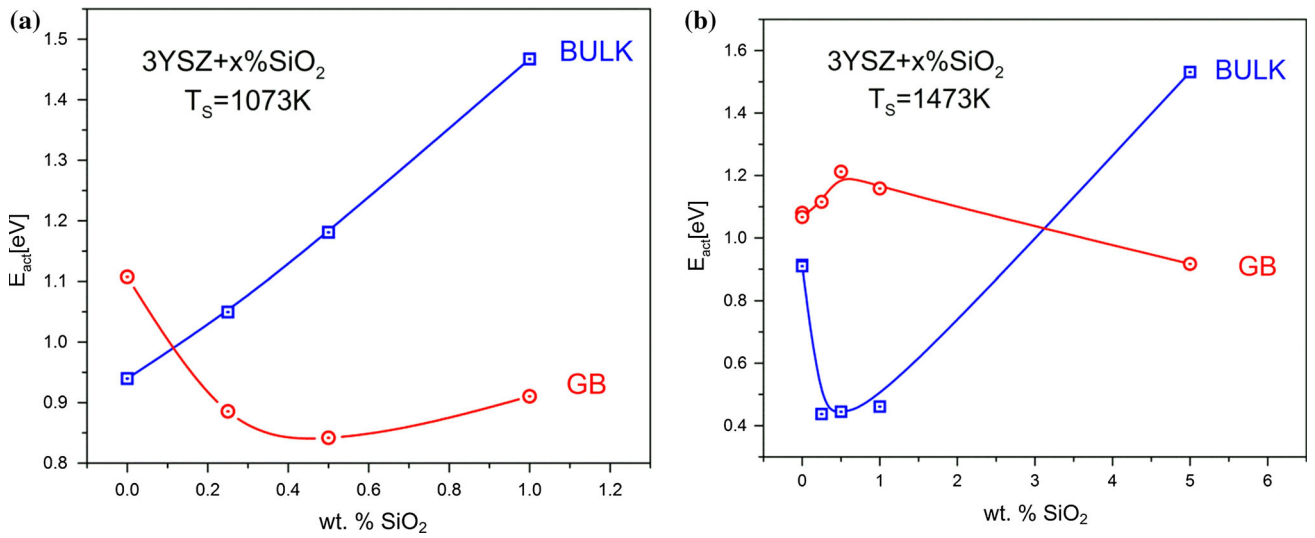

Figure 11 Activation energy versus SiO_2 concentration of the samples 3YSZ + xSiO_2; **a** samples sintered at 1073 K; **b** samples sintered at 1473 K.

mechanism of conductivity depending on the sintering temperatures (and therefore the microstructure) of the material. For the samples sintered at 1073 K, silica probably acts only as a medium for separating the 3YSZ grains (which prevents from the grains' growth) and as a medium which reduces the grain size. In the case of samples sintered at 1473 K, SiO_2 simultaneously acts as a medium which reduces grain size and also slightly reacts with YSZ (especially in the case of larger addition of SiO_2). The influence of silica dopant on the activation energy of grain interior conductivity (E_{act_b}) is actually opposite to that with respect to E_{act_gb}. For the samples slightly contaminated with silica and then sintered at 1473 K, the decrease of E_{act_b} can be noticed, while for the samples sintered at 1073 K, the significant increase in the values of E_{act_b} in the same range as that of SiO_2 amount is observed. It should be noted that in the case of 3YSZ + 0.25 wt% SiO_2 sintered at 1473 K, E_{act_b} assumes a very low value: 0.44 eV. This fact make this sample a promising candidate for IT-SOFC.

Conclusions

The effects of the additions of various amounts of silica and the influence of sintering temperature on both the microstructures of ZrO_2 containing 3 mol% Y_2O_3 (3YSZ) and its electrical properties have been studied. The microstructural investigation revealed that SiO_2 addition to 3YSZ leads to reduction in the sizes of zirconia grains. The impedance spectra analysis shows that the two factors reported in the literature have an influence on grain boundary conductivity—grain size and the amount of introduced silica. The samples heated at 1073 K reveal higher values of grain boundary conductivity than that of the samples sintered at 1473 K. This behaviour is a result of small grain sizes (therefore, low grain boundary resistance) of such obtained materials. In the case of samples sintered at 1473 K, the effect of glassy layer formation becomes competitive for pinning effect.

In conclusion, from the viewpoint of potential application of the tested 3YSZ system as a component of the composite anode material (or electrolyte material) for SOFC technology, a small impurity of silica (up to 0.5 wt%) in 3YSZ should not significantly affect the electrical properties of this system. What is more, for the fine grain-sized 3YSZ materials, small addition of SiO_2 should even improve the grain boundary conductivities of these materials in comparison with pure Y_2O_3-ZrO_2 system. Moreover, addition of silica to 3YSZ has beneficial effect, because it prevents grain growth at critical sizes more than ca. 0.3 μm, where tetragonal zirconia becomes unstable and undergoes phase transition to monoclinic.

Acknowledgements

This work was financially supported by the National Science Centre of the Republic of Poland, under Grant No 2014/14/E/ST5/00763.

Compliance with ethical standards

Conflict of interest The authors declare that they have no conflict of interest.

References

[1] Kobayashi K, Kawajima H, Masaki T (1981) Phase change and mechanical properties of ZrO_2-Y_2O_3 solid electrolyte after ageing. Solid State Ionics 3(4):489–793

[2] Gupta TK, Bechtold JH, Kuznick RC, Cadoff LH, Rossing BR (1977) Stabilization of tetragonal phase in polycrystalline zirconia. J Mater Sci 12:2421–2426. doi:10.1007/BF00553928

[3] Gupta TK, Grekila RB, Subbaro EC (1981) Electrical conductivity of tetragonal zirconia below the transformation temperature. J Electrochem Soc 128:929–931

[4] Garvie RC, Hannik RHJ, Pascoe RT (1975) Micromechanical study of the morphology of martensite in constrained zirconia. Nature 258:703–704

[5] Badwal SPS (1990) Yttria tetragonal zirconia polycrystalline electrolytes for solid state electrochemical cells. Appl Phys A 50:449–462

[6] Brown M, Primdahl S, Mogensen M (2000) Structure performance relations for Ni/yttria-stabilized zirconia anodes for solid oxide fuel cells. J Electrochem Soc 147(2):475–485

[7] Koide H, Someya Y, Yoshida T, Maruyama T (2000) Properties of Ni/YSZ cermet as anode for SOFC. Solid State Ionics 132(3–4):253–260

[8] Han MF, Tang XL, Yin HY, Peng SP (2007) Fabrication, microstructure and properties of a YSZ electrolyte for SOFCs. J Power Sources 165(2):757–763

[9] Badwal SPS, Drennan J (1989) Grain boundary resistivity in YTZP materials as a function of thermal history. J Mater Sci 24:88–96. doi:10.1007/BF00660937

[10] Bonanos N, Slotwinski RK, Steele BCH (1984) High ionic conductivity in polycrystalline tetragonal Y_2O_3–ZrO_2. J Mater Sci Lett 3:245–248. doi:10.1007/BF00726805

[11] Meyer D, Eisele U, Satet R, Rödel J (2008) Codoping of zirconia with yttria and scandia. Scripta Mater 58:215–2018

[12] Guo X, Zhang Z (2003) Grain size dependent grain boundary defect structure: case of doped zirconia. Acta Mater 51:2539–2547

[13] Rűhle M, Claussen N, Heuer AH (1984) Microstructural studies of Y_2O_3 containing tetragonal ZrO_2 polycrystals (Y-TZP). Adv Ceram 12:352–370

[14] Tanaka J, Baumard JF, Abelard P (1987) Nonlinear electrical properties of grain boundaries in an oxygen-ion conductor ($CeO_2 \times Y_2O_3$). J Am Ceram Soc 70:637–643

[15] Stoto T, Neuer M, Carry C (1991) Influence of residual impurities on phase partitioning and grain growth processes of Y-TZP materials. J Am Ceram Soc 74:2615–2621

[16] Badwal SPS (1995) Grain boundary resistivity in zirconia-based materials: effect of sintering temperatures and impurities. Solid State Ionics 76:67–80

[17] Pradhan SK, Sinha M (2005) Microstructure characterization of nanocrystalline $ZrSiO_4$ synthesized by ball-milling and high-temperature annealing. J Appl Crystallogr 38(6): 951–957

[18] Verkerk MJ, Winnubst AJA, Burggraaafm AJ (1982) Effect of impurities on sintering and conductivity of yttria-stabilized zirconia. J Mater Sci 17:3113–3122. doi:10.1007/BF01203473

[19] Hughes AE, Sexton BA (1989) XPS study of an intergranular phase in yttria-zirconia. J Mat Sci 24:1057–1061. doi:10.1007/BF01148798

[20] Guo X, Maier J (2001) Grain boundary blocking effect in zirconia: a Schottky barrier analysis. J Electrochem Soc 148:E121–E126

[21] Martin MC, Mecartney ML (2003) Grain boundary ionic conductivity of yttrium stabilized zirconia as a function of silica content and grain size. Solid State Ionics 161:67–69

[22] Butler EP, Slotwinski RK, Bonanos N, Drennan J and Steele BCH (1984) Advances in Ceramics: Science and Technology of Zirconia II. In Claussen N, Ruhle M, Heuer AH. American Ceramic Society, Columbus 12: 572-584

[23] Drożdż E, Wyrwa J, Rękas M (2013) Influence of sintering temperature and aging on properties of cermet Ni/8YSZ materials obtained by citric method. Ionics 19:1733–1743

[24] Ruff O, Ebert F (1929) The structure of crystals. Z. Anorg Chem 180, 1st Edition

[25] Stevens R, (1986) An introduction to zirconia ceramics. 2nd Ed Twickenham: Magnesium electrum (Magnesium Elektron Publications no 113)

[26] Hanawalt JD, Rinn HW, Frevel LK (1938) Chemical analysis by X-Ray diffraction. Indust Chem Anal Ed 10:475–512
[27] Shannon RD, Prewitt CT (1969) Effective ionic radii in oxides and fluorides. Acta Cryst. B25:925–946
[28] Mondal P, Klein A, Jeagermann W, Hahn H (1999) Enhanced specific grain boundary conductivity innanocrystalline Y_2O_3–stabilized zirconia. Solid State Ionics 118:331–339
[29] Weller M, Schubert H (1986) Internal friction, dielectric lossand ionic conductivity of tetragonal ZrO2–3 % Y2O3 (Y-TZP). J Am Ceram Soc 69:573–577
[30] Park K, Olander DR (1991) Oxygen diffusion in single-crystal tetragonal zirconia. J Electrochem Soc 138:1154–1159
[31] Kim BK, Park SJ, Hamaguchi H (1994) Raman spectroscopic determination of the oxygen self-diffusion coefficients in oxide. J Am Ceram Soc 77:2648–2652
[32] Bauerle JE (1969) Study of solid electrolyte polarization by a complex admittance method. J Phys Chem Solids 30:2657–2669
[33] Hirschorn B, Orazem ME, Tribollet B, Vivier V, Frateur I, Musiani M (2010) Determination of effective capacitance and film thickness from constant-phase-element parameters. Electrochim Acta 55:6218–6227
[34] Ikuhara Y, Yamamoto T, Kuwabara A, Yoshida H, Sakuma T (2001) Structure and chemistry of grain boundaries in SiO_2-doped TZP. Sci Technol Adv Mater 2:411–424
[35] Lee JS, Kim DY (2001) Space-charge concepts on grain boundary impedance of a high-purity yttria-stabilized tetragonal zirconia polycrystal. J Mater Res 16(9):2739–2751